# Real-Time Surface Plasmon Resonance Study of Biomolecular Interactions between Polymerase and Bulky Mutagenic DNA Lesions

Lifang Xu,[‡] V. G. Vaidyanathan,[†,‡] and Bongsup P. Cho*

Department of Biomedical and Pharmaceutical Sciences, College of Pharmacy, University of Rhode Island, Kingston, Rhode Island 02881, United States

S *Supporting Information*

ABSTRACT: Surface plasmon resonance (SPR) was used to measure polymerase-binding interactions of the bulky mutagenic DNA lesions N-(2′-deoxyguanosin-8-yl)-4′-fluoro-4-aminobiphenyl (FABP) or N-(2′-deoxyguanosin-8-yl)-7-fluoro-2-acetylaminofluorene (FAAF) in the context of two unique 5′-flanking bases ($\underline{C}$G*A and $\underline{T}$G*A). The enzymes used were exonuclease-deficient Klenow fragment (Kf-exo⁻) or polymerase β (pol β). Specific binary and ternary DNA binding affinities of the enzymes were characterized at subnanomolar concentrations. The SPR results showed that Kf-exo⁻ binds strongly to a double strand/single strand template/primer junction, whereas pol β binds preferentially to double-stranded DNA having a one-nucleotide gap. Both enzymes exhibited tight binding to native DNA, with high nucleotide selectivity, where the K_D values for each base pair increased in the order dCTP $\ll$ dTTP $\sim$ dATP $\ll$ dGTP. In contrast to that for pol β, Kf-exo⁻ binds tightly to lesion-modified templates; however, both polymerases exhibited minimal nucleotide selectivity toward adducted DNA. Primer steady-state kinetics and ^{19}F NMR results support the SPR data. The relative insertion efficiency f_{ins} of dCTP opposite FABP was significantly higher in the $\underline{T}$G*A sequence compared to that in $\underline{C}$G*A. Although Kf-exo⁻ was not sensitive to the presence of a DNA lesion, FAAF-induced conformational heterogeneity perturbed the active site of pol β, weakening the enzyme's ability to bind to FAAF adducts compared to FABP adducts. The present study demonstrates the effectiveness of SPR for elucidating how lesion-induced conformational heterogeneity affects the binding capability of polymerases and ultimately the nucleotide insertion efficiency.
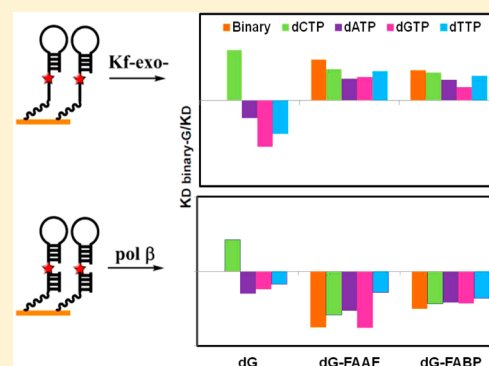
INTRODUCTION

Polymerases are critical to the replication and repair of DNA.[1] While replication of DNA is an essential first step for cell division, repair of DNA is needed when insults such as UV rays, environmental toxins, and some drugs chemically modify DNA.[2] These modifications can yield a diverse array of mutations.[3] To understand the mechanisms of DNA replication and repair, it is crucial to understand how a polymerase processes DNA lesions.[4,5]

As part of ongoing carcinogenesis research and to understand the mechanisms of DNA mutation and repair, we have been studying how the bulky and mutagenic arylamine−DNA lesions (Figure 1a) interact with a polymerase or a repair protein.[6−11] Using ^{19}F NMR, microcalorimetric, and other biophyisical methods, we have shown that the arylamine lesions adopt three unique conformations: base-displaced stacked (S), major groove B-type (B), and minor-groove wedge (W), depending on the location of the lesion (Figure 1b).[10−13] The relative populations of S-, B-, and W-conformers depend on the nature of attachment on the central nitrogen (N-acetyl vs N-deacetylated) and the hydrophobic carcinogen ring moiety (planar vs twisted) as well as the base sequences (flanking vs near long-range) surrounding the lesion.[13−15]

It has been shown that most replicative polymerases easily bypass the planar and N-deacetylated aminofluorene (AF) adducts after a brief stall at the lesion site. On the other hand, the bulkier N-(2′-deoxyguanosin-8-yl)-2-acetylaminofluorene (AAF) analogues cannot be readily bypassed and thus stall DNA synthesis.[16] In *in vitro* studies with X-family polymerase β, AAF adducts lead to −2 base deletion mutations, while AF extends full-length primers.[17] A recent study via single-molecule fluorescence spectroscopy showed that high-fidelity polymerases cannot extend a primer whose terminus occurs across from AAF.[18] In *E. coli*, AAF adducts result mostly in frameshift mutations, while both AF and AAF adducts cause point mutations.[19] In mammals, both adducts afford point mutations.[17] This difference in mutagenic profiles has been attributed to the presence of a bulky acetyl group on the central nitrogen, which causes the AAF adduct to adopt a *syn* conformation.[20] In contrast, the AF adduct adopts an *anti-/syn-* conformation, while the N-(2′-deoxyguanosin-8-yl)-4′-fluoro-4-aminobiphenyl (FABP) adduct adopts exclusively an *anti-* conformation.[9] Other factors influencing adduct-induced mutations include topology, insertion of the nucleotide
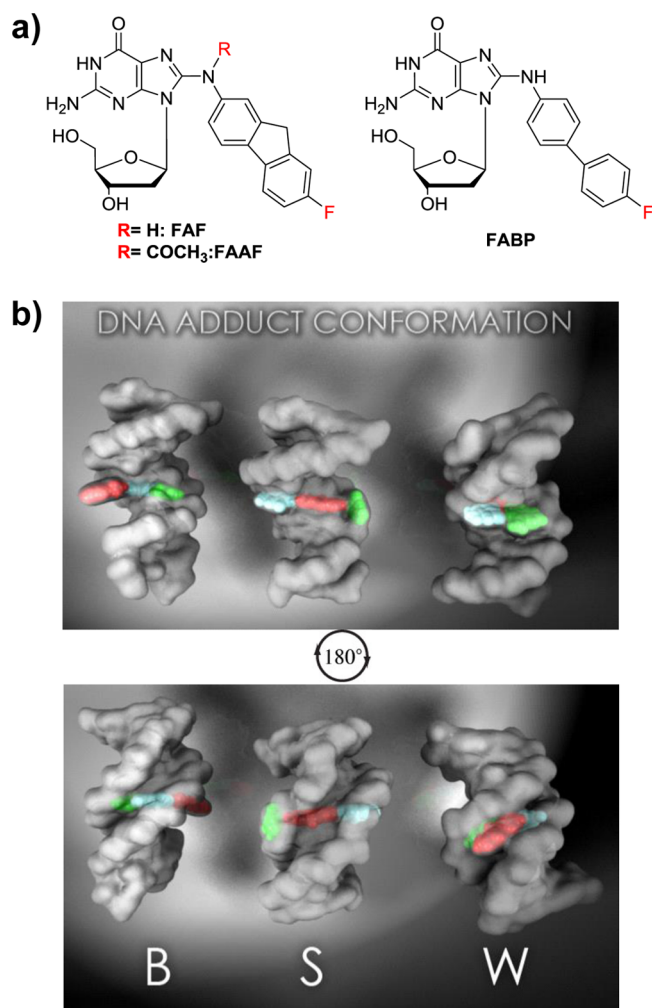
Figure 1. (a) Chemical structures of FAAF— and FABP—dG adducts. (b) Major (upper image) and minor (lower image) groove views of the prototype B-, S-, and W-conformers of arylamine—dG lesions in CPK model with the DNA duplex in gray surface (color code: arylamine lesion, red; modified-dG, cyan; dC opposite the lesion site, green). Note that the arylamine lesion (red) in W-conformation is wedged in the narrow minor groove.

opposite the lesion site, and the characteristics of the polymerase.[21,22]

Numerous crystal structure and kinetic analysis studies are available and provide information on actions of native[23−25] and damaged[2,5,26−34] DNA with various polymerases. However, only few examples of replicative polymerases complexed with bulky arylamine-modified DNA are available with atomic resolution details,[26,27] presumably due to difficulties with obtaining crystals. High-resolution solution NMR can offer dynamic information alternative to that of static crystallography.[35,36] However, some bulky DNA lesions cause conformational variation in the DNA that can also occur upon binding with a polymerase, which introduces additional challenges to the use of this method.[14,15,37−39] As a result, most NMR studies thus far are limited to adducted DNA without the full presence of polymerases and repair proteins.[40,41] Theoretical/molecular dynamic simulations in conjunction with limited NMR and crystal data have been useful.[4,40,42,43]

Other available techniques for biomolecular interactions such as electrophoretic mobility (gel shift or gel retardation assay) and filter-binding assays provide valuable information on binding affinity. However, these approaches contribute either little or no insight on the kinetic parameters underlying complex formation. Moreover, these techniques require strenuous work to determine binding parameters.[44] In addition, gel assays do not allow the samples of interest to be in chemical equilibrium due to fast dissociation rate during electrophoresis; thus, it is difficult to measure proper binding kinetics and thermodynamics.[44] Finally, microcalorimetry, such as isothermal titration calorimetry (ITC), is a fast and robust method that certainly could be used to characterize binding interactions and the thermodynamics of polymerase DNA interactions in free solution, but low-affinity interactions would require higher protein concentrations.[44]

Surface plasmon resonance (SPR) is a powerful, chip-based, and label-free solution technology that can provide real-time information on kinetics and thermodynamics.[44−48] SPR relies on changes in the refractive index that are due to changes in mass and can thus measure a small difference in binding (K_D) at the subnanomolar level. SPR is thus ideal for probing interactions of binary and ternary polymerase—DNA interactions. We have recently communicated our initial SPR work on the binding affinities of Kf-exo$^-$ to arylamine DNA lesions.[6,49] Subsequently, a similar study was conducted to elucidate how FAF lesions affect the active site conformation of the human repair enzyme pol β and how the structure and sequence of the DNA affects its ability to be repaired.[7]

In the present study, we are providing a complete set of SPR data on the binding of Kf-exo$^-$ or pol β to FAAF and FABP lesions in two different sequences (CG*A and TG*A). To complement the SPR binding results, we also conducted dynamic ^{19}F NMR as well as steady-state nucleotide insertion kinetics. The results are discussed in terms of adduct-induced conformational heterogeneity, the effect of the 5′-flanking base sequence, substrate specificity, and the nature of a polymerase. The purpose of the present article is 2-fold: (1) to give the full details of our previous SPR work[6] and (2) to introduce SPR to the chemical toxicology community as a powerful alternative to existing techniques for investigating protein—DNA interactions. As a result, the choice of polymerases used in the present study was based largely on the experimental systems in our previous work.[7,8,21] Obviously, future SPR studies should be expanded to a range of Y-family bypass polymerases, which are more likely to be involved in replication of bulky DNA lesions.

■ MATERIALS AND METHODS

DNA sequences containing 5′-biotin-labeled 31-mer oligonucleotides, phosphorylated 52-mer hairpin, and 21-mer complementary sequences (Figure 2b,c) were purchased from Operon (Eurofin, Huntsville, AL) in desalted form and purified by reverse-phase high-performance liquid chromatography (RP-HPLC). All HPLC solvents were purchased from Fisher Inc. (Pittsburgh, PA) and used as received. The HPLC system consisted of a Hitachi EZChrom Elite HPLC system with an L2450 diode array detector and a Clarity column (10 mm × 150 mm, 3 μm) (Phenomenex, Torrance, CA). The mobile phase system involved a 20 min linear gradient profile from 3 to 16% (v/v) acetonitrile with 100 mM ammonium acetate buffer (pH 6.5) at a flow rate of 2.0 mL/min. Kf-exo$^-$ (D424A) and pol β were received as gifts from Dr. Catherine Joyce (Yale University, New Haven, CT) and Dr. William Beard (NIEHS, Research Triangle Park, NC).
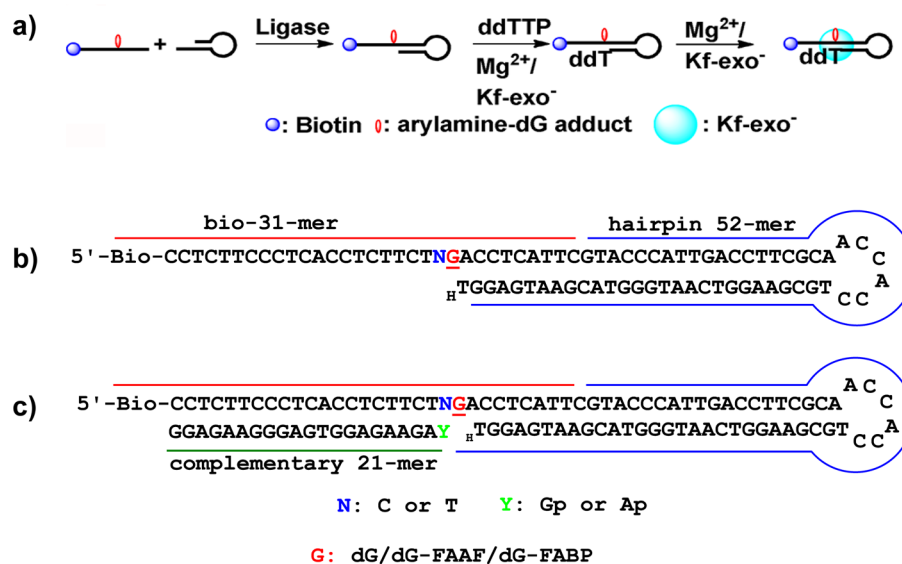
Figure 2. (a) Schematic representation of template−primer DNA constructs for SPR assays; hairpin template−primer oligonucleotide constructs for (b) Kf-exo⁻ and (c) pol β.

¹⁹F NMR. Approximately 70 μM of a FAAF− or FABP−dG modified 16-mer template was annealed with a 9-mer primer in a 1:1 molar ratio to produce a ds/ss junction containing duplexes (Figure 3). The samples were lyophilized and dissolved in 300 μL of typical pH 7.0 NMR buffer containing 10% D_2O/90% H_2O with 100 mM NaCl, 10 mM sodium phosphate, and 100 μM EDTA. All ¹⁹F NMR spectra were recorded using a dedicated 5 mm ¹⁹F/¹H dual probe on a Varian 500 MHz spectrometer operating at 476.5 MHz, using acquisition parameters described previously.[11,50,51] The spectra were acquired in the ¹H-decoupled mode and referenced relative to that of $CFCl_3$ by assigning external C_6F_6 in C_6D_6 at −164.9 ppm. ¹⁹F NMR spectra were measured at two different temperatures, 5 and 25 °C.

Primer Extension Assay. *Standing Start Experiments.* Single-nucleotide/full-length extension experiments for both FABP− and FAAF−dG adducts in Kf-exo⁻ were performed as described previously.[8] Briefly, the 9-mer primer was 5′-radiolabeled using [γ-³²P]ATP and T4 polynucleotide kinase (T4 PNK) following the manufacturer's protocol. The ³²P-labeled primer (50 pmol) was annealed with either an unmodified or adducted template oligonucleotide (60 pmol) by heating at 95 °C for 5 min and then slowly cooling to room temperature in 3 h. For pol β assays, a 1 nt gap was generated by adding a downstream 9-mer primer with 5′-phosphate group while annealing with radiolabeled primer (9-mer) and template (19-mer).[7] The ds/ss primer−template sequence (20 nM) was incubated with Kf-exo⁻ (0.5 or 1.0 nM) for 5 min to form a binary complex in Tris buffer (Tris, 50 mM, pH 7.4; BSA, 50 μg/mL; 5% (v/v) glycerol). The reaction was initiated by adding a dNTP (100 μM)/$MgCl_2$ (5 mM) solution to a binary mixture and was incubated at 22 °C for 10 min. The reaction was arrested with gel loading buffer (containing 50 mM EDTA (pH 8.0)/95% formamide solution). The quenched sample was heated at 95 °C for 5 min and immediately cooled on ice. The products were resolved with a denaturing polyacrylamide gel (20% polyacryamide (w/v)/7 M urea), electrophoresed at 2500 V for 4 h. The gel was exposed on a Kodak phosphor imaging screen overnight and scanned with a Typhoon 9410 variable mode imager.

Steady-State Kinetics Analysis. To determine the efficiency of dCTP insertion opposite the adducted site, steady-state kinetic parameters for incorporation of the nucleotide opposite the unmodified and FABP-modified templates were determined by using the reported literature procedures.[7,8] The reactions were performed with pol β (0.5 nM) and oligonucleotide (20 nM) at 22 °C. For the unmodified sequence, reactions were performed in a shorter time period of 0.5−10 min for nucleotide incorporation and up to 30 min in the case of modified templates. The band intensities were quantitated using ImageQuantTL from GE Healthcare. The percentage of primer extended in kinetic assays was determined by taking the ratio of extended primer to the total amount of primer (unextended + extended primer). The kinetic parameters k_{cat} and K_m were determined as described earlier.[7,8]

SPR Measurements. *Arylamine-Modified Hairpin Template/Primer Constructs.* The modification of 5′-biotin CGA/TGA sequences (31-mer) was carried out using the previously reported procedures (Figure 2),[6,7] and the modified products were purified by RP-HPLC and characterized by MALDI-TOF mass spectrometry. Biotinylated unmodified (20 μM) or modified 31-mer (20 μM) was annealed with 20 μM of 52-mer hairpin by heating at 95 °C for 5 min and cooling to room temperature (Figure 2). The annealed mixture was ligated by using 4000 U T4 DNA ligase in 1× ligase buffer for 16 h at room temperature. The ligated 83-mer oligonucleotide was purified by 10% denaturing polyacrylamide gel (Figure S1) and extracted using the crush and soak method. The extracted oligonucleotide was desalted using an Illustra G-25 spin column. The desalted oligonucleotide was incubated with 2′,3′-dideoxy-thymidine-5′-triphosphate (ddTTP) (1 mM) in the presence of Kf-exo⁻ (1 μM) and 5 mM $MgCl_2$ for 12 h. The dideoxy-terminus DNA was purified by RP-HPLC (Figure S2) after precipitation of protein using phenol−chloroform−isoamyl alcohol (25:24:1) followed by ethanol extraction.

Characterization of Oligonucleotides by MALDI-TOF. Either a biotinylated 31-, 83-, or 84-mer DNA sequence (100 pmol) was mixed with 2 μL of matrix containing 1 μL of 3-hydroxy picolinic acid (3-HPA) (50 mg/mL dissolved in acetonitrile/water 50% v/v) and 1 μL of diammonium

hydrogen citrate (DAHC) (50 mg/mL dissolved in acetonitrile/water 50% v/v). MALDI-TOF experiments were performed using Axima Performance from Shimadzu Biotech. The mass spectrometric measurement of 31-mer oligonucleotides was carried out in a reflectron positive mode. The calibration of the instrument in reflectron positive mode was performed using low-molecular-weight oligonucleotide or peptide standard calibration kit. For high-molecular-weight oligonucleotides (>10 000 Da), calibration was done in a linear negative mode using 52-, 80-, 90-, and 100-mer standards with laser power 120 in order to enhance the signal intensity. The spectral data was processed by using Shimadzu Biotech MALDI-MS software with processing parameters as follows: smoothing filter width as 20 channels, baseline filter width as 80 channels, and double threshold.

DNA Coating on Biosensor Chip. SPR measurements were conducted with Biacore T200 (GE Healthcare). A carboxymethylated dextran-coated CM5 chip supplied by GE Healthcare was used to immobilize streptavidin (SA) via the amine coupling kit on flow cells by following the previously reported literature.[6,7,49] The EDC/NHS mixture was injected over the surface for 7 min followed by SA (50 μg/mL dissolved in sodium acetate buffer, pH 4.5). The unreacted reactive esters were blocked with 1 M ethanolamine for 7 min. The running buffer used for immobilization was 1× HBS-EP$^+$ buffer containing 10 mM Hepes (pH 7.4), 150 mM NaCl, 3 mM EDTA, and 0.05% nonionic surfactant P20. The flow cells were immobilized with SA around 2500 RU. After SA immobilization, the surface was washed with 50 mM NaOH for 60 s pulse, which was repeated five times to remove the free SA until the change in response unit reached below 20 RU. The surface was stabilized by injecting (3−4 times) running buffer followed by equilibration with running buffer for 1 h. The 84-mer biotinylated DNA-hairpin sequences of either unmodified or adducted DNA (0.25−0.3 nM) were injected over the flow cells 2 or 4 for 60−120 s individually to achieve 0.7−3.5 RU. The flow cells were washed with running buffer to remove the unbound DNA and to stabilize the surface. Before conducting kinetics experiments, 1 mM ddTTP in the presence of Kf-exo$^-$ (1 μM) and 5 mM MgCl$_2$ was injected over the surface for 5 min followed by 0.05% SDS to remove the polymerase. For pol β experiments, a 1 nt gap was created by using the same DNA coating approach, and, in addition, a corresponding downstream complementary sequence (21-mer) containing a 5'-phosphate group (2 nM) was injected over the surface for 5 min.

Real-Time Kinetic Analysis. Kf-exo$^-$ was injected with or without dNTPs (100 μM) over the DNA surface in random order (neither ascending nor descending concentrations). Each concentration was repeated twice. For the binary system, varying concentrations of Kf-exo$^-$ (0−10 nM) prepared in running buffer containing 1× HBS-P$^+$ along with 100 μg/mL bovine serum albumin (BSA) and 5 mM MgCl$_2$ was used. The polymerase was injected for 30 s at a flow rate of 100 μL/min followed by dissociation of polymerase. The surface was regenerated using 0.05% SDS at a flow rate of 100 μL/min, and the injection time was 30 s followed by an extra wash with running buffer. After regeneration of the surface, the surface was stabilized with running buffer for 15 min. Initially, three startup steps with running buffer and four zero-concentration injections were performed to condition the surface. For the ternary system, individual dNTP (100 μM) was mixed with varying concentrations of Kf-exo$^-$ and injected over the surface.

The sensorgrams were double-referenced and fitted using a 1:1 Langmuir model. The binding affinity constants (K_D) for binary and ternary systems were calculated using steady-state affinity analysis in BIAevaluation software v1.0 as the association rate for the ternary system, particularly as dCTP and unmodified dG are near the diffusion limit. The sensorgrams for binary systems were globally fitted with BIAsimulation basic kinetics module software by using experimental k_a and k_d values (Figure S7).
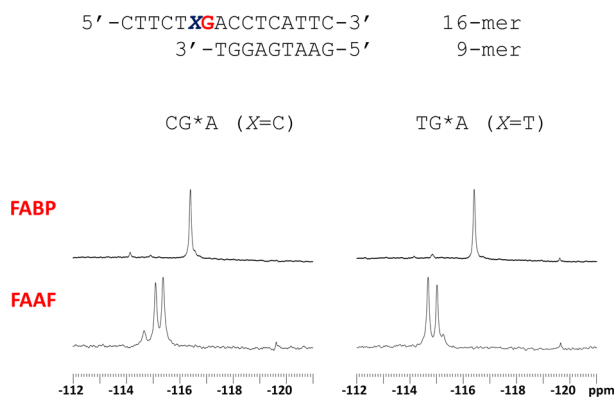
Similar experiments were carried out for pol β interaction studies with adduct present both at the nongapped duplex DNA and 1 nt gap DNA. Single-nucleotide (1 nt)-gapped DNA was generated by annealing a corresponding downstream primer. For nongapped DNA, the concentration of pol β was varied up to 1000 nM, whereas for 1 nt gap, it was 0−100 nM depending on the dG adduct embedded. The binding constants were obtained using a 1:1 Langmuir model.

■ RESULTS

Model Hairpin Template/Primer Constructs. An overall scheme for the construction of the biotinylated hairpin-based template−primer strands is depicted in Figure 2a. FABP- or FAAF-modified biotin-31-mer oligonucleotides were prepared according to published procedures.[7,10,12] The 52-mer hairpin DNA was annealed and ligated to the biotinylated 31-mer (Figure 2b, c). ddTTP was incorporated at the 3' primer's terminus using Kf-exo$^-$.[25,52] The hairpin structure was created to improve the thermal stability of the oligonucleotide constructs on a gold chip during kinetics experiments. As a result, the same oligonucleotide constructs could be used multiple times with different polymerases and buffer conditions. Finally, the lesion was positioned at the 22nd base, with 21 bases on the 5'-side and 28 bases on the 3'-side, in order to avoid close contact between the polymerase and the chip surface. The resulting template/primer strands, containing the biotinylated 84-mer hairpin, were purified by denaturing polyacrylamide gel (Figure S1) and used for further study.

MALDI-TOF spectrum, obtained in reflectron mode, of the FAAF-modified biotin-TG*A-31-mer sequence is shown in Figure S3. A distinctive peak at 9841.30 Da is in close agreement with theory (9839.90 Da, Δm/z: +1.40), and the inset is a linear negative mode spectrum. The inset b at 25925.76 Da corresponds to the 83-mer strand consisting of the biotin-31-mer-TG[FAAF]A- and the 52-mer hairpin in the absence of ddT at the primer terminus (theoretical 25923.00 Da, Δm/z: +2.76). The inset c at 26206.70 Da corresponds to the 84-mer strand formed by adding ddT to the primer terminus of the 83-mer strand (26211.00 Da, Δm/z: −4.30). The corresponding TG[FABP]A, CG[FAAF]A, and CG-[FABP]A sequences were similarly characterized (Figure S4−S6). All of the calculated and experimental m/z values are shown in Table S1.
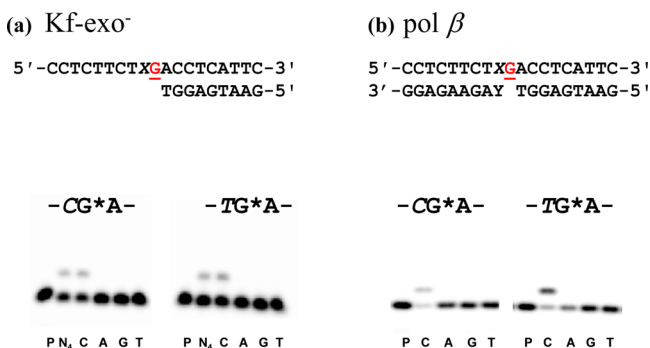
^{19}F NMR. To examine lesion-induced conformational heterogeneity, we measured ^{19}F NMR spectra of modified 16/9-mer template/primer duplexes. As shown in Figure 3, the ^{19}F NMR spectra of FABP- and FAAF-modified duplexes in the CG*A and TG*A sequences are compared at 25 °C. FABP duplexes exhibited a single peak at −116.4 ppm in both sequences, which is consistent with the chemical shift range observed previously for the *anti*-B-type FABP conformer.[9] The bulky FAAF displayed three ^{19}F signals, with two prominent peaks of similar intensity at around −114 to −116 ppm, for both sequences. We have previously reported the chemical shift ranges that correspond to the B-, S-, and W-conformers of

```
5'-CTTCTXGACCTCATTC-3'      16-mer
       3'-TGGAGTAAG-5'       9-mer
```

CG*A (X=C)   TG*A (X=T)

FABP

FAAF

-112 -114 -116 -118 -120   -112 -114 -116 -118 -120 ppm

Figure 3. ^{19}F NMR spectra of FABP and FAAF adducts in the CGA and TGA duplexes at a ds/ss junction at 25 °C.

FAAF-modified duplexes, i.e., −115.0 to −115.5 ppm for the B-conformer, −115.5 to −117.0 ppm for the S-conformer, and −117.0 to −118.0 ppm for the W-conformer.[11,13] Hence, the present FAAF-induced heterogeneity could be a variation of the B/S/W heterogeneity. In contrast to the aforementioned study, however, the ^{19}F signals in the present study are derived from the lesions at the ds/ss junction, not fully paired double helical duplexes.[8,12] The relative shielding of ^{19}F signals and the narrow chemical shift range (∼2 ppm) in the present work are probably due to the flexible lesions at the ds/ss junction. As a result, we could not unequivocally assign the signals to the B-, S-, or W-conformer.

Primer Extension Assay. Single-nucleotide incorporation was carried out using the *E. coli* exonuclease-deficient Klenow fragment (Kf-exo⁻) and the human base excision repair polymerase β (pol β) (Figure 4). Like any other high-fidelity

(a) Kf-exo⁻   **(b)** pol β

```
5'-CCTCTTCTXGACCTCATTC-3'    5'-CCTCTTCTXGACCTCATTC-3'
        TGGAGTAAG-5'          3'-GGAGAAGAY TGGAGTAAG-5'
```

−CG*A−   −TG*A−   −CG*A−   −TG*A−

PN₄CAGT   PN₄CAGT   PCAGT   PCAGT

Figure 4. Assays of full-length and single-nucleotide incorporation into FABP-adducted CG*A and TG*A sequences with (a) Kf-exo⁻ and (b) pol β.

replicative polymerase, Kf-exo⁻ prefers the ds/ss replication fork as a template/primer DNA substrate. In the unmodified DNA control, the primer was immediately elongated to full length in the presence of all four nucleotides and Kf-exo⁻ (data not shown). With the FABP-modified template, however, primer elongation was largely stalled at the lesion site, with some insertion of the correct dCTP opposite the lesion (Figure 4a).

Unlike Kf-exo⁻, pol β prefers a single-nucleotide gap as a substrate.[53,54] With pol β, there was no full extension of either the unmodified (not shown) or FABP-modified template (Figure 4b). We observed preferential dCTP incorporation opposite the lesion. As for FAAF, no nucleotide insertion was observed with either Kf-exo⁻ or pol β, even at high enzyme concentrations or with a longer incubation period (data not shown), because the lesion had completely blocked elongation.

Steady-State Kinetics. We conducted steady-state experiments to investigate the impact of conformational heterogeneity on nucleotide insertion kinetics. The results for Kf-exo⁻ and pol β are summarized in Tables 1 and 2, respectively. To examine the influence of lesions, we used the relative insertion efficiency f_{ins}, which was defined as $(k_{cat}/K_m)_{modified\ or\ mismatched}$ $/(k_{cat}/K_m)_{unmodified}$. With Kf-exo⁻, the f_{ins} of dCTP opposite -CG[FABP]A- was 500-fold lower than that of the unmodified control (Table 1). This is contrasted with -TG[FABP]A-, which was reduced only 33-fold. In the pol β assay (Table 2), the f_{ins} of dCTP opposite FABP in the CGA sequence was 142-fold lower than that of the control, while in the TGA sequence, the f_{ins} was 59-fold lower than that of the control. These results indicate that the nucleotide insertion efficiency is consistently greater in the TGA sequence compared to that in the CGA sequence, regardless of the polymerase structure. We were unable to perform similar steady-state kinetics experiments for FAAF because this lesion caused a major blockage at the replication fork.

SPR Binding Experiments. *DNA Coating and Mass Transport Limitation Studies.* After activation with streptavidin (SA), flow cells 1 and 3 were retained as blank references, and DNA was coated on the SA surface of flow cells 2 and 4. Surface testing, regeneration buffer scouting, and the mass transport limitation test were performed before the kinetics experiments, as described previously.[6] DNA coating at 0.7 resonance units (RU) did not show any influence of mass transport; an increase in flow rate of the analyte did not alter the association rate. However, at 10 RU, mass transport became a limiting factor, as the association rate deviated with the flow rate of the analyte (data not shown). On the basis of this study of mass transport limitation, all of the experiments were carried out in the DNA coating range between 0.7 and 3.5 RU.

Kf-exo⁻. The sensorgrams for the binary binding between Kf-exo⁻ and the unmodified TGA controls or the modified TG*A oligonucleotide constructs are shown in Figure 5a. We performed steady-state affinity analysis of the binary and ternary complexes in the presence of four dNTPs (Figure 6). A similar set of results for the CGA sequence have been reported

**Table 1. Steady-State Kinetics Parameters for Insertion of dCTP Opposite Unmodified and FABP−dG Adduct with Kf-exo⁻**

sequence context	incoming dNTP	k_{cat} (min⁻¹)	$K_{m,dCTP}$ (μM)	k_{cat}/K_m (μM⁻¹ min⁻¹)	$f_{ins}{}^a$
-C**G**A-	dCTP	21.9(1.4)	0.80 (0.24)	27.3(8.4)	1.00
-CG[**FABP**]A-	dCTP	0.44(0.05)	6.62(3.37)	0.06(0.03)	0.002
-T**G**A-	dCTP	3.10(0.31)	0.23(0.14)	13.8(8.3)	1.00
-TG[**FABP**]A-	dCTP	0.32(0.02)	0.66(0.30)	0.48(0.22)	0.03

$^a f_{ins} = (k_{cat}/K_m)_{modified}/(k_{cat}/K_m)_{unmodified\ dG\ control}$.

Table 2. Steady-State Kinetics Parameters for Insertion of dCTP Opposite Unmodified and FABP−dG Adduct 1 nt Gap with Pol β

sequence context	incoming dNTP	k_{cat} (min^{-1})	$K_{m,dCTP}$ (μM)	k_{cat}/K_m (μM^{-1} min^{-1})	f_{ins}[a]
-C**G**A-	dCTP	1.14(0.08)	1.98(0.73)	0.58(0.21)	1.00
-C**G**[**FABP**]A-	dCTP	0.60(0.09)	135(41)	0.004(0.001)	0.007
-T**G**A-	dCTP	0.83(0.06)	4.75(1.48)	0.17(0.05)	1.00
-T**G**[**FABP**]A-	dCTP	1.02(0.14)	298(69)	0.003(0.001)	0.017

[a]$f_{ins} = (k_{cat}/K_m)_{modified}/(k_{cat}/K_m)_{unmodified\ dG\ control}$.
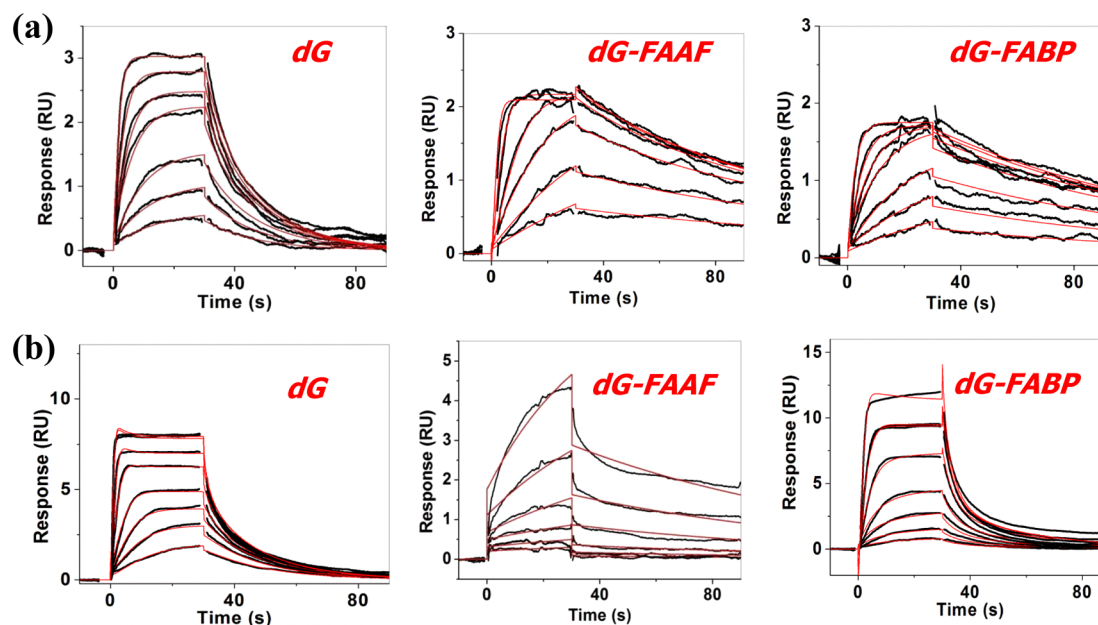
Figure 5. Sensorgrams of binary complexes of (a) Kf-exo⁻ and (b) pol β with unmodified and modified TGA sequences (1:1 binding fitted curves are overlaid as red lines).
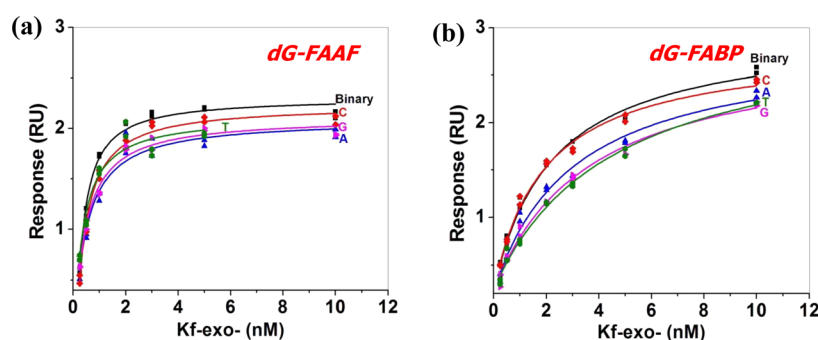
Figure 6. Steady-state affinity analysis of interaction of Kf-exo⁻ with (a) -TG[FAAF]A- and (b) -TG[FABP]A- sequences.

Table 3. SPR Binding Affinities $(K_D)^a$ of Unmodified TGA/CGA and Arylamine−dG Adducts with Kf-exo⁻ (Steady-State Affinity Analysis) in the Binary and Ternary Systems

sequence	binary	dCTP	dATP	dGTP	dTTP
-T**G**A-	1.3(0.3)	0.09(0.08)	3.5(1.1)	16(8)	3.60(0.95)
-C**G**A-[b]	1.5(0.5)	0.05(0.02)	3.1(2.2)	13(12)	1.70(0.53)
-T**G**[**FAAF**]A-	0.15(0.05)	0.25(0.06)	0.42(0.18)	0.38(0.10)	0.28(0.19)
-C**G**[**FAAF**]A-[b]	0.21(0.05)	0.19(0.11)	0.33(0.05)	0.67(0.07)	0.43(0.08)
-T**G**[**FABP**]A-	0.27(0.02)	0.30(0.03)	0.44(0.01)	0.66(0.08)	0.36(0.07)
-C**G**[**FABP**]A-[b]	0.14(0.10)	0.29(0.12)	0.31(0.13)	0.63(0.11)	0.54(0.17)

$^a K_D$ values are in nanomolar (nM). $^b K_D$ values were taken from ref 6.

previously,[6] and the results on the binding affinity of Kf-exo⁻ to both TGA and CGA sequences are summarized in Table 3.

As for the unmodified controls, Kf-exo⁻ binds tightly in both sequences in the presence of the correct dCTP. The affinity of

Table 4. SPR Binding Affinities (K_D)^a of Unmodified TGA/CGA and Arylamine–dG Adducts with Pol β (1:1 Binding) in the Binary and Ternary Systems^b

sequence	binary	dCTP	dATP	dGTP	dTTP
-T**G**A-	0.80(0.17)	0.30(0.09)	1.6(0.3)	1.40(0.15)	1.2(0.2)
-C**G**A-	0.90(0.10)	0.20(0.12)	2.10(0.09)	2.10(0.09)	1.8(0.2)
-T**G**[**FAAF**]A-	4.50(0.15)	3.10(0.16)	2.70(0.09)	4.60(0.12)	1.50(0.04)
-C**G**[**FAAF**]A-	5.20(0.12)	4.40(0.08)	3.7(0.1)	1.90(0.05)	1.10(0.21)
-T**G**[**FABP**]A-	2.60(0.25)	2.20(0.23)	2.10(0.17)	2.20(0.16)	1.80(0.12)
-C**G**[**FABP**]A-	2.80(0.21)	1.80(0.08)	2.00(0.08)	2.10(0.07)	1.80(0.06)

$^a K_D$ values are in nanomolar (nM). ^{b}For nongapped duplex DNA (ds-DNA) with pol β, K_D values exceeds 0.8 μM.

binding for the CGA sequence was reduced by 30-, 62-, 264-, and 34-fold in binary, dATP, dGTP, and dTTP, respectively, compared to that for the correct dCTP binding (Table 3). Similar results were obtained for TGA, where the binding affinity was reduced by 15-, 39-, 180-, and 40-fold in binary, dATP, dGTP, and dTTP, respectively (Table 3). These results are consistent with those of the nucleotide insertion assay, which showed preferential insertion of the correct dCTP.

Kf-exo$^-$ bound strongly to the modified TG*A templates. In the TG*A sequence, the K_D value for FABP was 4.9-fold greater than that of the control, and the K_D value for FAAF was 8.8-fold greater than that of the control. Similar changes were observed in the CG*A sequence, where the K_D for FABP was 10.8-fold larger than that for the control, and the K_D for FAAF was 7.2-fold larger than that for the control. These differences are primarily due to the much slower dissociation rates observed for the modified template/primer for both the CG*A sequence (FAAF k_d: 0.02 s^{-1}; FABP k_d: 0.01 s^{-1}) and the TG*A sequence (FAAF k_d: 0.01 s^{-1}; FABP k_d: 0.01 s^{-1}). The net stabilization energies were positive and ranged from 1.10 to 1.47 kcal/mol (Table S2).

Nucleotide selectivity was low in the modified ternary complexes. K_D for the correct nucleotide was 0.19–0.25 nM with FAAF and 0.29–0.30 nM with FABP, while for the incorrect nucleotide, K_D was 0.28–0.67 nM with FAAF and 0.31–0.66 nM with FABP.

Pol β. For pol β, binding assays were performed on two distinct substrates: nongapped ds/ss and 1 nt gap. The results for the binary and ternary systems on both CGA and TGA sequences are summarized in Table 4. Weak binding was observed for the nongapped DNA, with K_D values of ~0.8 μM (data not shown). In contrast, the binding affinity of pol β increased 1000-fold with the 1 nt gap.

As for the unmodified controls, pol β binds to the correct dCTP more tightly. The binding affinity for the dCTP is 2.7-fold higher in the TGA sequence and 4.5-fold higher in the CGA sequence (Table 4). In contrast to Kf-exo$^-$, the binding in the binary complex between the modified template and pol β is less tight than that in the complex containing the unmodified template, where the differences in binding are approximately 3-fold for FABP and 5- to 6-fold for FAAF, respectively. Similar to Kf-exo$^-$, the binary complex with FAAF showed slower off rates (k_d: 0.01 s^{-1}) with pol β in both sequences. The curve fits for dG–FAAF (Figure 5b) are relatively poor; however, the residual plots for the dG–FAAF/pol β binary complex (Figure S10) indicate a good curve fit within 1% χ^2 values of R_{max}. The complexes with B-conformeric FABP exhibited unusually faster dissociation rates for both the CG*A and TG*A sequences, where the k_d values were 0.76 and 0.40 s^{-1}, respectively, and the negative net stabilization energy was −1.04 and −0.27 kcal/mol, respectively (Table S2).

Figure S9 shows the sensorgrams for the ternary complexes between pol β and the FAAF- and FABP-modified CG*A constructs. We have recently reported a similar set of binding results for the N-deacetylated FAF.[7] With the correct nucleotide dCTP, the pol β binds 2.7-fold more tightly in the ternary complex than that in the binary complex and ~3000-fold more tightly than to that of nongapped DNA. The binding affinity to the incorrect nucleotide was 4- to 5-fold lower than that to the correct dCTP. The lesion in the 1 nt gap reduced the binding affinity of pol β by 6-fold for FAAF and 3-fold for FABP, virtually eliminating the nucleotide selectivity of pol β at the lesion site. The affinity for pol β binding decreased in the order dG > FABP > FAAF.

DISCUSSION

In the present study, we have employed SPR to investigate the binary and ternary binding interactions of Kf-exo$^-$ and pol β to two prototype arylamine–DNA lesions (FABP and FAAF) in the context of two different sequences (CG*A and TG*A). Kf-exo$^-$ is a 68 kDa high-fidelity replicative A-family bacterial DNA polymerase,[55] which carries polymerase and 3′−5′ exonuclease activities and has been used extensively as a model enzyme for studying adduct-induced DNA synthesis. Pol β is the smallest (39 kDa) eukaryotic polymerase, belonging to the X-family of base excision repair DNA polymerases, and has been characterized extensively.[56] With pol β, primer extension past AAF adduct was blocked, but full-length products were shown to contain exclusively −2 deletion mutations.[17] Although its role is limited in base excision repair, pol β has been additionally implicated in the replication of various DNA damage. For example, deregulation of pol β may enhance the genetic instability induced by bulky lesions such as cisplatin[32] and UV radiation.[33] Pol β can also bypass abasic sites[57] and bulky polyaromatic hydrocarbon adducts.[34] FABP and FAAF are C8-substituted dG adducts that contain structurally unique arylamine structures, i.e., N-acetylated/coplanar-fluorene and N-deacetylated/twisted-biphenyl, respectively (Figure 1a). Finally, the two sequences (C**G***A vs T**G***A) were selected because of their marked difference in the S/B population ratios observed with the N-deacetylated FAF.[11] The SPR results, along with data from ^{19}F NMR and steady-state primer kinetics, elucidate how lesion-induced conformational heterogeneity alters the binding capacity of a polymerase and thus its nucleotide insertion efficiency.

Model Hairpin Oligonucleotide Constructs for SPR Binding Assays. We constructed the 84-mer hairpin-based oligonucleotides for SPR (Figure 2) based on the following considerations. First, the incorporation of ddT at the 3′-end of the primer prevents the usual nucleophilic attack of the 3′-hydroxyl to the incoming dNTP and thus blocks the formation of a phosphodiester bond.[25,58] This ensures the stability of the

ternary complex polymerase/template-primer/dNTP for SPR measurements. Previous assays using gel electrophoresis, single-molecule FRET, or crystallography have consistently shown that the absence of 3′-OH at the primer terminus does not affect the affinity with which polymerases bind to binary and ternary complexes of DNA.[25,58] Second, while Kf-exo⁻ requires a minimum of 11 bases, because it covers approximately 5 bases downstream from the primer/template junction and 6 to 7 bases upstream of the 3′-primer's terminus,[59] pol β can operate on any length of DNA containing a 1 nt gap.

Binary and Ternary Binding Affinities with Unmodified Control DNA. We observed very tight binding of Kf-exo⁻ with native unmodified dG in the presence of the correct incoming nucleotide dCTP. This system exhibited high nucleotide selectivity, with K_D values increasing in the order dCTP $\ll$ dTTP $\sim$ dATP $\ll$ dGTP (Table 3). The SPR results are in agreement with nucleotide insertion assays, which showed exclusive insertion of the correct dCTP over other dNTPs. Crystal structures usually indicate 1:1 DNA polymerase−DNA complexes. 2:1 and higher order complexes have also been observed in solution by various biochemical and biophysical methods.[59] The stoichiometry, however, is highly concentration-dependent. As shown in Figure S11, comparison between theoretical and experimental R_{max} for pol β and Kf-exo⁻ are in good agreement, indicating a 1:1 complex.

Initially, we carried out a SPR binding assay of pol β using the nongapped ds/ss junction replication fork. The binding was very weak, with K_D values in the micromolar concentration range.[7] However, upon introduction of the 1 nt gap (Figure 2c), the DNA binding affinity of pol β increased 200- to 1000-fold. These results indicate that the presence of 5′-PO₄ enhances the binding affinity of the 8 kDa lyase domain as well as the 31 kDa catalytic domain. The observed differences in binding affinity are consistent with previous reports in which the lyase domain in the duplex (nongapped) DNA was flexible. Introduction of the 1 nt gap enhances the binding affinity of the polymerase to DNA.[60] The results are also in agreement with gel assays, which have previously shown that addition of the correct dCTP opposite unmodified DNA enhances the binding affinity of polymerase compared to that with other nucleotides by an induced-fit model adopted by pol β.[60]

Lesion and Sequence Effects on Binary Binding Affinities with Modified DNA. An unusually greater binding of Kf-exo⁻ was observed for modified dG, where the K_D of this interaction was 5−11-fold higher than the K_D for interaction with the unmodified native DNA substrate. The binary binding affinity decreased in the order FABP > FAAF > dG for the CG*A sequence and FAAF > FABP > dG for the TG*A sequence (Table 3). Previous studies have also shown tighter binary binding of Kf-exo⁻ with the AAF adduct.[61] Using gel-retardation assays, Dzantiev and Romano[61] showed that the bulky and hydrophobic AAF interacts with nearby hydrophobic amino acid residues, strengthening its binding to the active site of Kf-exo⁻. The authors suggested that such lesion-induced conformational adjustment may block the conformational change required to properly accommodate an incoming nucleotide.[27]

It is well-established that the N-deacetylated fluorinated analogue FAF adducts (Figure 1) adopt sequence-dependent equilibrium between B- and S-conformers. FABP is similarly N-deacetylated, but it lacks a methylene bridge, resulting in a bulky twisted biphenyl moiety.[21] In other words, FABP may behave like FAAF at the replication fork of the template in the

active site of a polymerase. In contrast to the unmodified control, modified adducts displayed a significant decrease (7−13-fold) in dissociation rate, with positive net stabilization energy (Table S2). The markedly slower off rates are consistent with single-molecule FRET studies as well as gel shift assays in which the presence of the bulky DNA adduct stabilizes the binary complex and does not induce dissociation before nucleotide incorporation.[18,60]

In contrast to Kf-exo⁻, pol β exhibited significantly less binary binding affinity to the modified templates. Furthermore, the modified sequences exhibited significantly faster dissociation rates and more negative net stabilization energies. As in the ds/ss situation discussed above, it is likely that FAAF promotes conformational heterogeneity in a sequence containing a 1 nt gap. Such heterogeneity may hinder the interaction of that sequence with key amino acids in the polymerase, thus preventing the polymerase from undergoing conformational change that is necessary for strong binding.

Lesion and Sequence Effects on Ternary Binding Affinities with Modified DNA. Nucleotide selectivity was low in the ternary complexes with Kf-exo⁻, where the K_D values indicate poor discrimination between the correct (K_D 0.19−0.30 nM) and incorrect (K_D 0.28−0.67 nM) nucleotides. Variance in these values ranged from 1.5- to 3.5-fold (Table 3). This poor selectivity does not depend on the nature of the lesion (FABP vs FAAF) or the 5′-flanking base (CG*A vs TG*A). The lack of nucleotide selectivity appears to be in agreement with the results of tryptic digestion studies, in which the AAF−polymerase complex maintains an unstable non-catalytic open conformation in the presence of any dNTP.[62] In other words, AAF modification did not stabilize the complexes in relation to the incoming nucleotide. This is contrasted with native DNA, to which the polymerase binds very tightly in the presence of the correct nucleotide dCTP and is insensitive to digestion. Our ¹⁹F NMR results (Figure 3) indicate a complex conformational heterogeneity of the bulky FAAF at the ds/ss templating position, which may prevent the polymerase from properly accommodating an incoming dNTP. This reasoning is in accord with the weak electron densities observed for the arylamine base in the active site of T7 DNA polymerase,[27] where the authors of the previous study also concluded that conformational heterogeneity may hinder the insertion of an incoming nucleotide.

The low selectivity for incoming nucleotides could also arise from the high stability of the binary complex, which may hinder the polymerase's ability to recognize the incoming nucleotide. No crystal structures or high-resolution NMR structures are currently available for complexes between any DNA polymerase and ABP or the fluorinated FABP. In the present study, FABP in both sequences exhibited a single ¹⁹F signal, possibly for a B- or a B/S-conformational mix, owing to the presumed conformational flexibility at the ds/ss junction. These NMR data, albeit in the absence of a polymerase, are in agreement with the gel-based kinetics data, which reveal a preference toward inserting the correct nucleotide over other nucleotides (Table 1).

In the case of Kf-exo⁻, the TG*A sequence favored the insertion of dCTP more efficiently than the CG*A sequence. The relative insertion efficiency f_{ins} of dCTP opposite FABP was significantly lower in the CG*A (500-fold) and TG*A (33-fold) sequences compared to that of the unmodified controls (Table 1). This 15-fold difference in f_{ins} is puzzling because FABP at the ds/ss junction exhibited a single ¹⁹F signal in both
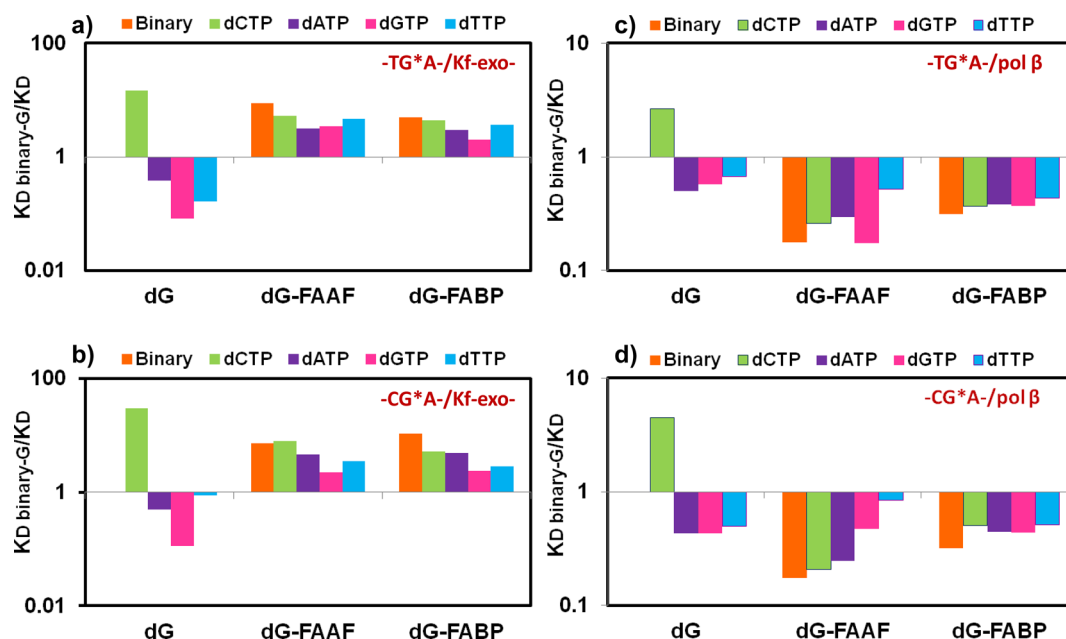
Figure 7. Plots of nucleotide specificity ratio (K_D-binary/K_D) with (a, b) Kf-exo⁻ and (c, d) pol β for unmodified and modified TG*A and CG*A DNA templates. The dNTPs are color-coded in the plots. K_D-binary-dG represents K_D of unmodified DNA-polymerase binary complex, and denominator K_D represents the ternary complex of unmodified DNA (or) binary and ternary complexes of adducted DNA.

sequences (Figure 3). However, we have shown previously that FAF in the duplex setting displayed a greater S-conformer in the CG*A duplex (50%) relative to that in TG*A (38%). As mentioned above, it is likely that the absence of coplanarity in FABP would embrace intermediate structures between FAAF and FAF, as observed from ¹⁹F NMR, gel, and SPR assays.

The SPR results with pol β (Table 4) indicated that a modified templating base weakens the polymerase's binding affinity and the nucleotide selectivity (Figure S9, Table 4). The reduced binding affinity of pol β to the modified template DNA could be related to the lesion-induced conformational heterogeneity in the active site of the polymerase. In the closed conformation, key amino acids such as Lys 234 and Tyr 271 interact with the minor groove of the primer strand, while Arg 283 interacts with the template strand of DNA. As mentioned above, it is possible that the FAAF at the 1 nt gap may hinder the active site geometry and thus prevent the conformational change necessary to form the catalytic ternary complex. We previously observed similar conformational heterogeneity caused by FAF bound to 1 nt gap DNA in both the absence and presence of pol β.[7] The results are also consistent with translesion synthesis studies in which the minor groove conformation benzo[*a*]pyrene diol epoxide−*N*²-dG adducts creates steric clash with the active site of pol β, thereby reducing the insertion rate.[63] These results are in agreement with the steady-state kinetics data that show significant reductions in the f_{ins} of dCTP opposite FABP in the CG*A and TG*A sequences (142- and 59-fold, respectively), relative to that of the corresponding unmodified controls.

The question is how to reconcile the apparent lack of discrimination between dNTP at the binding step (Figure 7 and Tables 3 and 4) with the clear preference for accurate insertion of dCTP (Figure 4 and Tables 1 and 2). We have recently shown that the AF adduct can change its binding characteristics at the replication fork or in a single-nucleotide gap in the active sites of DNA polymerases.[7] Similarly, it is

plausible that the dynamics of FABP- and FAAF-induced conformational heterogeniety could be altered to accommodate an incoming dNTP within the active site of polymerases in a way that favors the incorporation of the correct base dCTP.

SPR as a Powerful Tool for Probing Polymerase Action. In the present study, we have taken advantage of the sensitivity of SPR, which allowed us to probe the delicate interaction between polymerases and DNA strands containing arylamine−DNA lesions at the binary and ternary complex levels. We were able to measure a subnanomolar difference in binding affinity among dNTPs. We found that 0.7−3.5 RU of DNA coating was sufficient, with no significant interference from mass transport limitation.

The binding specificity ratios (K_D of the control binary complex over the K_D of a ternary complex) in the presence of dNTPs for the unmodified (dG) and FAAF- and FABP-modified lesions are plotted in Figure 7. The dNTPs are color-coded in the plot. We observed highly specific binding between Kf-exo⁻ and the native DNA substrates in the presence of the correct dCTP (green) opposite a dG templating base (Figure 7a,b). This is consistent with the polymerase undergoing a conformational change, from open to closed, to form Watson−Crick base pairs. Kf-exo⁻ binds weakly with the incorrect dNTPs, probably retaining the catalytically incompetent open conformation. The binding of dGTP (pink) with Kf-exo⁻ was particularly poor. Similar binding results were obtained with pol β (Figure 7c,d), although the affinities for modified ternary complexes were generally weaker than those with Kf-exo⁻. In both enzymes, however, we observed no discernible nucleotide specificity (dNTPs) and sequence effects (CG*A vs T*GA).

K_D values for the ternary complexes for unmodified DNA were determined using affinity analysis because the association rate (k_a) reaches the near-diffusion limit in native DNA. This procedure allowed for the monitoring of interactions between unmodified or adducted DNA with different polymerases on a single chip. The present work also demonstrates the utility of SPR in distinguishing the substrate preference of different

polymerases (e.g., ds/ss vs 1 nt gap for pol β). To our knowledge, this is the first comprehensive use of SPR to probe nucleotide insertion kinetics during the action of a polymerase. Furthermore, the present SPR work advances the limits of SPR technology,[48,64] demonstrating that SPR can measure subnanomolar affinity differences between incoming nucleotides and the active site of a polymerase.

In conclusion, we have characterized the SPR binding affinity of the mutagenic FABP and FAAF lesions bound to Kf-exo⁻ and pol β. Kf-exo⁻ binds strongly to ds/ss template/primer DNA, whereas pol β prefers gapped DNA. Tighter binding was observed between unmodified dG and Kf-exo⁻ or pol β. The systems exhibited nucleotide selectivity, with K_D values increasing in the order of dCTP ≪ dTTP ∼ dATP ≪ dGTP. Unlike pol β, Kf-exo⁻ binds tightly to both FAAF and FABP lesions in the binary systems. With lesion-modified templates, both polymerases exhibited minimal nucleotide selectivity. The relative insertion efficiency f_{ins} of dCTP opposite FABP was significantly higher in the TG*A sequence compared to that in the CG*A sequence and the unmodified controls. While the lesion effect was not significant in Kf-exo⁻, the active site of pol β is sensitive to the FAAF-induced conformational heterogeneity. Our SPR data are complemented by primer steady-state kinetics and ^{19}F NMR data and provide valuable insights into how lesion-induced conformational heterogeneity in DNA alters the action of polymerases and thus affects the nucleotide insertion efficiency and coding potential.

ASSOCIATED CONTENT

Ⓢ Supporting Information

Details of sample preparation, MALDI characterization, sensorgram simulation and binding kinetics; denature gel separation of ligated and nonligated oligonucleotides (Figure S1); HPLC chromatography of 83- and 84-mer TG[FAAF]A modified sequences (Figure S2); MALDI-TOF characterization of TG[FAAF]A 31-, 83-, and 84-mer (Figure S3), TG[FABP]A (Figure S4), CG[FAAF]A (Figure S5), and CG[FABP]A (Figure S6); fitted and simulated curves of TG[FABP]A with Kf-exo⁻ binding (Figure S7); sensorgrams of ternary Kf-exo⁻ complexed with TGA (Figure S8); sensorgrams of ternary pol β complexed with CGA (Figure S9); sensorgram and fitted residuals of pol β binding with FAAF-dG (Binary) (Figure S10); theoretical calculations of binding ratio (Figure S11); tabulated values for spectral data of arylamine modified 31- and 84-mer (Table S1); and kinetics details of sequence binding with Kf-exo⁻ and pol β in binary system (1:1 binding) (Table S2). This material is available free of charge via the Internet at http://pubs.acs.org.

AUTHOR INFORMATION

Corresponding Author

*Phone: +1 401 874 5024. Fax: +1 401 874 5766. E-mail: bcho@uri.edu.

Present Address

[†](V.G.V.) Chemical Laboratory, CSIR-CLRI, Adyar, Chennai 600020, India.

Author Contributions

[‡]L.X. and V.G.V. contributed equally to this work.

ABBREVIATIONS

FABP, N-(2′-deoxyguanosin-8-yl)-4′-fluoro-4-aminobiphenyl; FAAF, N-(2′-deoxyguanosin-8-yl)-7-fluoro-2-acetylaminofluorene; Kf-exo⁻, Klenow fragment exonuclease deficient; pol β, human DNA polymerase β; SPR, surface plasmon resonance

REFERENCES

(1) Delagoutte, E. (2012) DNA polymerases: mechanistic insight from biochemical and biophysical studies. *Front. Biosci., Landmark Ed.* 17, 509−544.

(2) Federley, R. G., and Romano, L. J. (2010) DNA polymerase: structural homology, conformational dynamics, and the effects of carcinogenic DNA adducts. *J. Nucleic Acids*, 457176.

(3) Kozack, R., Seo, K. Y., Jelinsky, S. A., and Loechler, E. L. (2000) Toward an understanding of the role of DNA adduct conformation in defining mutagenic mechanism based on studies of the major adduct (formed at N²-dG) of the potent environmental carcinogen, benzo[*a*]pyrene. *Mutat. Res.* 450, 41−59.

(4) Broyde, S., Wang, L., Rechkoblit, O., Geacintov, N. E., and Patel, D. J. (2008) Lesion processing: high-fidelity versus lesion-bypass DNA polymerases. *Trends Biochem. Sci.* 33, 209−219.

(5) Freisinger, E., Grollman, A. P., Miller, H., and Kisker, C. (2004) Lesion (in)tolerance reveals insights into DNA replication fidelity. *EMBO J.* 23, 1494−1505.

(6) Vaidyanathan, V. G., Xu, L., and Cho, B. P. (2012) Binary and ternary binding affinities between exonuclease-deficient Klenow fragment (Kf-exo⁻) and various arylamine DNA lesions characterized by surface plasmon resonance. *Chem. Res. Toxicol.* 25, 1568−1570.

(7) Vaidyanathan, V. G., Liang, F., Beard, W. A., Shock, D. D., Wilson, S. H., and Cho, B. P. (2013) Insights into the conformation of aminofluorene−deoxyguanine adduct in a DNA polymerase active site. *J. Biol. Chem.* 288, 23573−23585.

(8) Vaidyanathan, V. G., and Cho, B. P. (2012) Sequence effects on translesion synthesis of an aminofluorene−DNA adduct: conformational, thermodynamic, and primer extension kinetic studies. *Biochemistry* 51, 1983−1995.

(9) Jain, V., Hilton, B., Lin, B., Patnaik, S., Liang, F., Darian, E., Zou, Y., Mackerell, A. D., Jr., and Cho, B. P. (2013) Unusual sequence effects on nucleotide excision repair of arylamine lesions: DNA bending/distortion as a primary recognition factor. *Nucleic Acids Res.* 41, 869−880.

(10) Meneni, S., Shell, S. M., Zou, Y., and Cho, B. P. (2007) Conformation-specific recognition of carcinogen-DNA adduct in *Escherichia coli* nucleotide excision repair. *Chem. Res. Toxicol.* 20, 6−10.

(11) Meneni, S. R., Shell, S. M., Gao, L., Jurecka, P., Lee, W., Sponer, J., Zou, Y., Chiarelli, M. P., and Cho, B. P. (2007) Spectroscopic and theoretical insights into sequence effects of aminofluorene-induced conformational heterogeneity and nucleotide excision repair. *Biochemistry* 46, 11263−11278.

(12) Meneni, S., Liang, F., and Cho, B. P. (2007) Examination of the long-range effects of aminofluorene-induced conformational heterogeneity and its relevance to the mechanism of translesional DNA synthesis. *J. Mol. Biol.* 366, 1387−1400.

(13) Patnaik, S., and Cho, B. P. (2010) Structures of 2-acetylaminofluorene modified DNA revisited: insight into conformational heterogeneity. *Chem. Res. Toxicol.* 23, 1650−1652.

(14) Cho, B. P. (2010) Structure−function charateristics of aromatic amine−DNA adducts, in *The Chemical Biology of DNA Damage* (Geacintov, N. E., and Broyde, S., Eds.) pp 217−233, Wiley-VCH, Weinheim, Germany.

(15) Cho, B. P. (2004) Dynamic conformational heterogeneities of carcinogen−DNA adducts and their mutagenic relevance. *J. Environ. Sci. Health, Part C: Environ. Carcinog. Ecotoxicol. Rev. 22*, 57−90.

(16) Michaels, M. L., Johnson, D. L., Reid, T. M., King, C. M., and Romano, L. J. (1987) Evidence for *in vitro* translesion DNA synthesis past a site-specific aminofluorene adduct. *J. Biol. Chem. 262*, 14648−14654.

(17) Shibutani, S., Suzuki, N., and Grollman, A. P. (1998) Mutagenic specificity of (acetylamino)fluorene-derived DNA adducts in mammalian cells. *Biochemistry 37*, 12034−12041.

(18) Vrtis, K. B., Markiewicz, R. P., Romano, L. J., and Rueda, D. (2013) Carcinogenic adducts induce distinct DNA polymerase binding orientations. *Nucleic Acids Res. 41*, 7843−7853.

(19) Shibutani, S., Suzuki, N., Tan, X., Johnson, F., and Grollman, A. P. (2001) Influence of flanking sequence context on the mutagenicity of acetylaminofluorene-derived DNA adducts in mammalian cells. *Biochemistry 40*, 3717−3722.

(20) O'Handley, S. F., Sanford, D. G., Xu, R., Lester, C. C., Hingerty, B. E., Broyde, S., and Krugh, T. R. (1993) Structural characterization of an *N*-acetyl-2-aminofluorene (AAF) modified DNA oligomer by NMR, energy minimization, and molecular dynamics. *Biochemistry 32*, 2481−2497.

(21) Jain, V., Vaidyanathan, V. G., Patnaik, S., Gopal, S., and Cho, B. P. (2014) Conformational insights into the lesion and sequence effects for arylamine-induced translesion DNA synthesis: ^{19}F NMR, surface plasmon resonance, and primer kinetic studies. *Biochemistry 53*, 4059−4071.

(22) Seo, K.-Y., Jelinsky, S. A., and Loechler, E. L. (2000) Factors that influence the mutagenic patterns of DNA adducts from chemical carcinogens. *Mutat. Res. 463*, 215−246.

(23) Korolev, S., Nayal, M., Barnes, W. M., Di Cera, E., and Waksman, G. (1995) Crystal structure of the large fragment of *Thermus aquaticus* DNA polymerase I at 2.5-A resolution: structural basis for thermostability. *Proc. Natl. Acad. Sci. U.S.A. 92*, 9264−9268.

(24) Doublie, S., and Ellenberger, T. (1998) The mechanism of action of T7 DNA polymerase. *Curr. Opin. Struct. Biol. 8*, 704−712.

(25) Pelletier, H., Sawaya, M. R., Kumar, A., Wilson, S. H., and Kraut, J. (1994) Structures of ternary complexes of rat DNA polymerase beta, a DNA template-primer, and ddCTP. *Science 264*, 1891−1903.

(26) Hsu, G. W., Kiefer, J. R., Burnouf, D., Becherel, O. J., Fuchs, R. P. P., and Beese, L. S. (2004) Observing translesion synthesis of an aromatic amine DNA adduct by a high-fidelity DNA polymerase. *J. Biol. Chem. 279*, 50280−50285.

(27) Dutta, S., Li, Y., Johnson, D., Dzantiev, L., Richardson, C. C., Romano, L. J., and Ellenberger, T. (2004) Crystal structures of 2-acetylaminofluorene and 2-aminofluorene in complex with T7 DNA polymerase reveal mechanisms of mutagenesis. *Proc. Natl. Acad. Sci. U.S.A. 101*, 16186−16191.

(28) McAuley-Hecht, K. E., Leonard, G. A., Gibson, N. J., Thomson, J. B., Watson, W. P., Hunter, W. N., and Brown, T. (1994) Crystal structure of a DNA duplex containing 8-hydroxydeoxyguanine-adenine base pairs. *Biochemistry 33*, 10266−10270.

(29) Efrati, E., Tocco, G., Eritja, R., Wilson, S. H., and Goodman, M. F. (1999) "Action-at-a-distance" mutagenesis. 8-Oxo-7, 8-dihydro-2′-deoxyguanosine causes base substitution errors at neighboring template sites when copied by DNA polymerase beta. *J. Biol. Chem. 274*, 15920−15926.

(30) Hoffmann, J. S., Pillaire, M. J., Garcia-Estefania, D., Lapalu, S., and Villani, G. (1996) *In vitro* bypass replication of the cisplatin−d(GpG) lesion by calf thymus DNA polymerase beta and human immunodeficiency virus type I reverse transcriptase is highly mutagenic. *J. Biol. Chem. 271*, 15386−15392.

(31) Hoffmann, J. S., Pillaire, M. J., Maga, G., Podust, V., Hubscher, U., and Villani, G. (1995) DNA polymerase beta bypasses *in vitro* a single d(GpG)−cisplatin adduct placed on codon 13 of the HRAS gene. *Proc. Natl. Acad. Sci. U.S.A. 92*, 5356−5360.

(32) Canitrot, Y., Cazaux, C., Frechet, M., Bouayadi, K., Lesca, C., Salles, B., and Hoffmann, J. S. (1998) Overexpression of DNA polymerase beta in cell results in a mutator phenotype and a decreased sensitivity to anticancer drugs. *Proc. Natl. Acad. Sci. U.S.A. 95*, 12586−12590.

(33) Servant, L., Cazaux, C., Bieth, A., Iwai, S., Hanaoka, F., and Hoffmann, J. S. (2002) A role for DNA polymerase beta in mutagenic UV lesion bypass. *J. Biol. Chem. 277*, 50046−50053.

(34) Batra, V. K., Shock, D. D., Prasad, R., Beard, W. A., Hou, E. W., Pedersen, L. C., Sayer, J. M., Yagi, H., Kumar, S., Jerina, D. M., and Wilson, S. H. (2006) Structure of DNA polymerase beta with a benzo[*c*]phenanthrene diol epoxide-adducted template exhibits mutagenic features. *Proc. Natl. Acad. Sci. U.S.A. 103*, 17231−17236.

(35) Pustovalova, Y., Maciejewski, M. W., and Korzhnev, D. M. (2013) NMR mapping of PCNA interaction with translesion synthesis DNA polymerase Rev1 mediated by Rev1-BRCT domain. *J. Mol. Biol. 425*, 3091−3105.

(36) Berlow, R. B., Swain, M., Dalal, S., Sweasy, J. B., and Loria, J. P. (2012) Substrate-dependent millisecond domain motions in DNA polymerase beta. *J. Mol. Biol. 419*, 171−182.

(37) Geacintov, N. E., Cosman, M., Hingerty, B. E., Amin, S., Broyde, S., and Patel, D. J. (1997) NMR solution structures of stereoisometric covalent polycyclic aromatic carcinogen−DNA adduct: principles, patterns, and diversity. *Chem. Res. Toxicol. 10*, 111−146.

(38) Cho, B. P., Beland, F. A., and Marques, M. M. (1994) NMR structural studies of a 15-mer DNA duplex from a ras protooncogene modified with the carcinogen 2-aminofluorene: conformational heterogeneity. *Biochemistry 33*, 1373−1384.

(39) Patel, D. J., Mao, B., Gu, Z., Hingerty, B. E., Gorin, A., Basu, A. K., and Broyde, S. (1998) Nuclear magnetic resonance solution structures of covalent aromatic amine−DNA adducts and their mutagenic relevance. *Chem. Res. Toxicol. 11*, 391−407.

(40) Broyde, S., Wang, L., Zhang, L., Rechkoblit, O., Geacintov, N. E., and Patel, D. J. (2008) DNA adduct structure−function relationships: comparing solution with polymerase structures. *Chem. Res. Toxicol. 21*, 45−52.

(41) Lukin, M., and de Los Santos, C. (2006) NMR structures of damaged DNA. *Chem. Rev. 106*, 607−686.

(42) Tang, Y., Liu, Z., Ding, S., Lin, C. H., Cai, Y., Rodriguez, F. A., Sayer, J. M., Jerina, D. M., Amin, S., Broyde, S., and Geacintov, N. E. (2012) Nuclear magnetic resonance solution structure of an N^2-guanine DNA adduct derived from the potent tumorigen dibenzo-[*a,l*]pyrene: intercalation from the minor groove with ruptured Watson−Crick base pairing. *Biochemistry 51*, 9751−9762.

(43) Mu, H., Kropachev, K., Wang, L., Zhang, L., Kolbanovskiy, A., Kolbanovskiy, M., Geacintov, N. E., and Broyde, S. (2012) Nucleotide excision repair of 2-acetylaminofluorene- and 2-aminofluorene-(C8)-guanine adducts: molecular dynamics simulations elucidate how lesion structure and base sequence context impact repair efficiencies. *Nucleic Acids Res. 40*, 9675−9690.

(44) Dey, B., Thukral, S., Krishnan, S., Chakrobarty, M., Gupta, S., Manghani, C., and Rani, V. (2012) DNA−protein interactions: methods for detection and analysis. *Mol. Cell. Biochem. 365*, 279−299.

(45) Stengel, G., and Knoll, W. (2005) Surface plasmon field-enhanced fluorescence spectroscopy studies of primer extension reactions. *Nucleic Acids Res. 33*, e69.

(46) Sedletska, Y., Culard, F., Midoux, P., and Malinge, J. M. (2013) Interaction studies of muts and mutl with DNA containing the major cisplatin lesion and its mismatched counterpart under equilibrium and nonequilibrium conditions. *Biopolymers 99*, 636−647.

(47) Lebbink, J. H., Fish, A., Reumer, A., Natrajan, G., Winterwerp, H. H., and Sixma, T. K. (2010) Magnesium coordination controls the molecular switch function of DNA mismatch repair protein MutS. *J. Biol. Chem. 285*, 13131−13141.

(48) Ritzefeld, M., and Sewald, N. (2012) Real-time analysis of specific protein−DNA interactions with surface plasmon resonance. *J. Amino Acids*, 816032.

(49) Vaidyanathan, V. G., Xu, L., and Cho, B. P. (2013) Binding kinetics of DNA−protein interaction using surface plasmon resonance. *Protoc. Exchange*, DOI: 10.1038/protex.2013.1054.

(50) Jain, N., Li, Y., Zhang, L., Meneni, S. R., and Cho, B. P. (2007) Probing the sequence effects on NarI-induced −2 frameshift mutagenesis by dynamic ^{19}F NMR, UV, and CD spectroscopy. *Biochemistry 46*, 13310−13321.

(51) Jain, N., Meneni, S., Jain, V., and Cho, B. P. (2009) Influence of flanking sequence context on the conformational flexibility of aminofluorene-modified dG adduct in dA mismatch DNA duplexes. *Nucleic Acids Res. 37*, 1628−1637.

(52) Doublie, S., Sawaya, M. R., and Ellenberger, T. (1999) An open and closed case for all polymerases. *Structure 7*, R31−35.

(53) Singhal, R. K., and Wilson, S. H. (1993) Short gap-filling synthesis by DNA polymerase β is processive. *J. Biol. Chem. 268*, 15906−15911.

(54) Beard, W. A., and Wilson, S. H. (2000) Structural design of a eukaryotic DNA repair polymerase: DNA polymerase β. *Mutat. Res. 460*, 231−244.

(55) Derbyshire, V., Grindley, N. D., and Joyce, C. M. (1991) The 3′−5′ exonuclease of DNA polymerase I of *Escherichia coli*: contribution of each amino acid at the active site to the reaction. *EMBO J. 10*, 17−24.

(56) Beard, W. A., and Wilson, S. H. (2006) Structure and mechanism of DNA polymerase β. *Chem. Rev. 106*, 361−382.

(57) Efrati, E., Tocco, G., Eritja, R., Wilson, S. H., and Goodman, M. F. (1997) Abasic translesion synthesis by DNA polymerase β violates the "A-rule". Novel types of nucleotide incorporation by human DNA polymerase β at an abasic lesion in different sequence contexts. *J. Biol. Chem. 272*, 2559−2569.

(58) Doublie, S., Tabor, S., Long, A. M., Richardson, C. C., and Ellenberger, T. (1998) Crystal structure of a bacteriophage T7 DNA replication complex at 2.2 Å resolution. *Nature 391*, 251−258.

(59) Tang, K. H., and Tsai, M. D. (2008) Structure and function of 2:1 DNA polymerase. DNA complexes. *J. Cell. Physiol. 216*, 315−320.

(60) Ahn, J., Kraynov, V. S., Zhong, X., Werneburg, B. G., and Tsai, M. D. (1998) DNA polymerase β: effects of gapped DNA substrates on dNTP specificity, fidelity, processivity and conformational changes. *Biochem. J. 331*, 79−87.

(61) Dzantiev, L., and Romano, L. J. (1999) Interaction of *Escherichia coli* DNA polymerase I (Klenow fragment) with primer-templates containing *N*-acetyl-2-aminofluorene or *N*-2-aminofluorene adducts in the active site. *J. Biol. Chem. 274*, 3279−3284.

(62) Dzantiev, L., and Romano, L. J. (2000) Differential effects of *N*-acetyl-2-aminofluorene and N-2-aminofluorene adducts on the conformational change in the structure of DNA polymerase I (Klenow fragment). *Biochemistry 39*, 5139−5145.

(63) Chary, P., Beard, W. A., Wilson, S. H., and Lloyd, R. S. (2012) DNA polymerase β gap-filling translesion DNA synthesis. *Chem. Res. Toxicol. 17*, 2744−2754.

(64) Schlachter, C., Lisdat, F., Frohme, M., Erdmann, V. A., Konthur, Z., Lehrach, H., and Glokler, J. (2012) Pushing the detection limits: the evanescent field in surface plasmon resonance and analyte-induced folding observation of long human telomeric repeats. *Biosens. Bioelectron. 31*, 571−574.